THE IMPACT OF ANGLE PARAMETERISATION ON TERRESTRIAL LASER SCANNER SELF-CALIBRATION

D. D. Lichti

Department of Geomatics Engineering, The University of Calgary, 2500 University Dr NW, Calgary AB T2N 1N4
Canada – ddlichti@ucalgary.ca

Commission V, WG V/3

KEY WORDS: Calibration, Error, Laser Scanning, LIDAR, TLS

ABSTRACT:

The angular fields of view in which a terrestrial laser scanner captures data differ according to instrument construction. Both the so-called panoramic and hybrid instruments scan through a full horizontal field of view but their vertical fields of view can differ considerably in terms of range and mode of data acquisition. The differences in operational mode govern the allowable range for each of the two angular observables, namely the horizontal direction and the elevation angle, and, ultimately, their parameterisation as observation equations. The impact of the angle parameterisation on the quality of terrestrial laser scanning instrument self-calibration has been studied. Specifically, the correlation between the scanner orientation angles and the collimation axis error coefficient, whose estimation in terrestrial laser scanner self-calibration has been reported to be unreliable as a result of this mechanism, was examined. It is been demonstrated with both simulated and real data that the angle parameterisation used for hybrid-type scanners is not only the cause of unreliable collimation axis error estimation but is also the reason for the reported ineffectiveness of certain self-calibration network design measures, notably the capture of scans having orthogonal orientations from the same nominal location

1. INTRODUCTION

An important aspect of the quality assurance of three-dimensional point clouds captured with terrestrial laser scanning (TLS) instruments is geometric calibration. Systematic errors inherent to such instruments can, if not corrected, degrade the accuracy of point clouds captured with a scanner. Systematic error modelling and a corresponding calibration procedure for estimating the model coefficients are therefore necessary. Furthermore, the calibration procedure must be as tractable as possible so that the time and effort required to perform it are minimal.

Self-calibration approaches have recently been investigated by a number of researchers and can be categorised according to the type of targeting used. Two types are reported: signalised point targets and planar features. The common thread between both approaches is the collection of a highly redundant set of spherical observations (range, horizontal direction and elevation angle) from different locations in a strong geometric configuration. The model variables comprising the scanner position and angular orientation elements, the target parameters (point co-ordinates or plane parameters) and the systematic error coefficients, called the additional parameters (APs), are estimated from these observations. Point-target approaches have been used for the calibration of various TLS systems by Abmayr et al. (2005), Lichti (2007), Reshetyuk (2006, 2009) and Schneider and Schwalbe (2008). TLS self-calibration using planar features has been reported by Gielsdorf et al. (2004), Bae and Lichti (2007) and Dorninger et al. (2008).

The advantages of the self-calibration approach include optimal estimation of all model variables and that no special equipment or facilities, such as an electronic distance meter baseline, are required except for a room comprising some form of targeting.

It can yield very precise APs that have been demonstrated, through independent assessment, to improve the accuracy of subsequently-acquired point cloud data (e.g. Lichti, 2007). While one goal of self-calibration network design is to reduce the functional dependence between model variables, the mitigation of some correlation mechanisms remains problematic and is the subject of ongoing investigation.

This paper focuses primarily on the mitigation of the correlation between the collimation axis error and the scanner orientation angles, which is reported to cause unreliable estimation of this important systematic error model term (e.g., Reshetyuk 2006, 2009; Schneider and Schwalbe, 2008). The present study demonstrates, through the self-calibration of both simulated and real data, that the means chosen to parameterise the angular observations has a significant impact on this correlation mechanism and on the precision of certain angular systematic error coefficients. Moreover, it is shown that the angle parameterisation is the reason why certain self-calibration network design features, specifically the capture of scans having orthogonal orientations from the same nominal location, are judged to be ineffective (e.g. Reshetyuk, 2009).

This paper commences with a discussion of different instrument architectures, which dictate how scanner data are captured and, subsequently, how the angle observations are parameterised. Next, the observation modelling for point-target self-calibration and the accompanying systematic error models are described. These necessary background subjects are followed by a more detailed discussion of the parameter correlation problem at hand. A set of simulations, designed to show how the correlation mechanism in question manifests itself and how it can be reduced, are then described and the results analysed. Results from real datasets that confirm the simulation findings then follow.

2. TLS MODELLING

2.1 Scanner Architectures

Following the terminology of Staiger (2003), TLS instruments can be categorised as either a camera scanner, having a limited field of view (FOV) of, say, 40° x 40°, a panoramic scanner or a hybrid scanner. This work is concerned with the latter two, which are capable of scanning through a full horizontal FOV. The panoramic and hybrid scanners differ in terms of their scanning mechanisms and their vertical fields of view. Scanning in the horizontal direction is performed by rotation of the instrument head about its vertical axis for both types. A panoramic scanner rotates through a horizontal range of 180° and features a rotating, single-facet mirror on the end of a shaft that deflects the laser beam from a lower vertical limit of a few tens of degrees above nadir, α_0, up through zenith and down again to the lower limit. Data are thus captured in front of and behind the instrument along each vertical scanning profile. The so-called first and second layers correspond to data below the zenith and data above the zenith, respectively (Abmayr et al., 2005). The entire field of view scanned is spherical save for a small cone beneath the instrument. Examples of panoramic scanners include the Faro LS 880 and the Leica HDS 6000, which have respective vertical fields of view of 320° and 310° (POB, 2009).

A hybrid scanner rotates through a horizontal range of 360° and acquires data in a vertical FOV that ranges from a minimum value below the instrument's horizontal plane, α_{min}, to some maximum value, α_{max}, which may be the zenith direction (i.e. 90°). It features either a rotating polygonal mirror (e.g., the Riegl LMS-Z620) or an oscillating mirror (e.g., the Trimble GX 3D Scanner), which provide smaller vertical fields of view of 80° and 60°, respectively (POB, 2009). The Leica ScanStation 2 also uses oscillating mirrors. Its vertical FOV extends up to the zenith by virtue of scanning through two separate windows (one on the front, one on the top). Though its coverage is nearly spherical, like a panoramic scanner, it is classified as a hybrid scanner due its construction and its 360° horizontal angular range. The rotation angle ranges for both the horizontal (θ) and vertical (α) observables of each scanner category are summarised in Table 1.

Scanner Architecture	Horizontal rotation range	Vertical rotation range
Panoramic	$0 < \theta < 180°$	$\alpha_0 < \alpha < 270° - \alpha_0$
Hybrid	$0 < \theta < 360°$	$\alpha_{min} < \alpha < \alpha_{max}$

Table 1. Rotation ranges of panoramic and hybrid TLS instruments.

2.2 Point Target Observation Models

The observation of a point i from scanner location j can be expressed in terms of range, ρ_{ij}, horizontal direction, θ_{ij}, and elevation angle, α_{ij},

$$\rho_{ij} + \varepsilon_{\rho_{ij}} = \sqrt{x_{ij}^2 + y_{ij}^2 + z_{ij}^2} + \Delta\rho \tag{1}$$

$$\theta_{ij} + \varepsilon_{\theta_{ij}} = \arctan\left(\frac{y_{ij}}{x_{ij}}\right) + \Delta\theta \tag{2}$$

$$\alpha_{ij} + \varepsilon_{\alpha_{ij}} = \arctan\left(\frac{z_{ij}}{\sqrt{x_{ij}^2 + y_{ij}^2}}\right) + \Delta\alpha \tag{3}$$

where $(x, y, z)_{ij}$ are the Cartesian co-ordinates of point i in scanner-space j, which is related to object space by the rigid body transformation

$$\begin{bmatrix} x_{ij} \\ y_{ij} \\ z_{ij} \end{bmatrix} = R_3(\kappa_j)R_2(\phi_j)R_1(\omega_j)\left\{ \begin{bmatrix} X_i \\ Y_i \\ Z_i \end{bmatrix} - \begin{bmatrix} X_{s_j} \\ Y_{s_j} \\ Z_{s_j} \end{bmatrix} \right\} \tag{4}$$

$(X, Y, Z)_i$ and $(X_s, Y_s, Z_s)_j$ the object-space co-ordinates of point i and scanner location j, respectively; $(\omega, \phi, \kappa)_j$ are the rotation angles from object space to scanner space j that, coupled with the scanner location co-ordinates, comprise the elements of exterior orientation; R_1, R_2, R_3 are the matrices for rotation about the X-, Y- and Z-axes, respectively; $\Delta\rho$, $\Delta\theta$ and $\Delta\alpha$ represent the respective systematic error correction models for the observations; and the ε terms represent the respective random errors.

If the scanner can be levelled via two orthogonal inclinometers, then the following two parameter observations can be written for each scan location

$$\omega_j + \varepsilon_{\omega_j} = 0 \tag{5}$$

$$\phi_j + \varepsilon_{\phi_j} = 0 \tag{6}$$

One of the benefits of including these observations is the de-correlation of these angles from the vertical circle index error (Lichti, 2007).

Naturally, the observation equations developed for TLS instruments should model the acquisition geometry as closely as possible, which includes the scanner data extents. The values of θ and α calculated in a self-calibration adjustment can quite easily be refined with conditional software statements to lie in the correct angular ranges according to the mode of data capture as indicated in Table 1.

2.3 Additional Parameter Models

Guided by similarities in construction to theodolites and total stations, TLS systematic error model selection is driven by the requirements for a particular instrument, i.e. model identification from highly-redundant datasets. The following models, comprising the rangefinder offset or additive constant, a_0, the collimation axis error, b_1, the trunnion axis error, b_2, and the vertical circle index error, c_0, can quite reasonably be described as a basic set of APs for TLS instruments.

$$\Delta\rho = a_0 \tag{7}$$

$$\Delta\theta = b_1 \sec(\alpha_{ij}) + b_2 \tan(\alpha_{ij}) \tag{8}$$

$$\Delta\alpha = c_0 \tag{9}$$

The rangefinder offset a_0 models the offset between the range measurement origin and the scanner space origin. The

collimation axis error b_1 is the non-orthogonality between the instrument's collimation and horizontal (trunnion) axes. It is constant for horizontal elevation angles, i.e. $\alpha=0°$ and $\alpha=180°$. For elevation angles greater than 90°, this error has the same magnitude as it does for angles less than 90° but with opposite sign. The trunnion axis error b_2 is the non-orthogonality between the scanner's trunnion and vertical axes. It is zero for horizontal elevation angles. The vertical circle error c_0 models the constant offset between the scanner-space horizontal plane and the elevation angle measurement origin.

Though more extensive sets of APs are reported in the literature, this constitutes a common set of parameters in the models of Gielsdorf et al. (2004), Lichti (2007), Reshetyuk (2006, 2009) and Schneider and Schwalbe (2008). Additionally, the models of Abmayr et al. (2005) include the latter three parameters. These four terms can also be described as the basic parameters of total station instruments, which share many salient properties with TLS instruments in terms of their construction and can be self-calibrated in a similar manner (Lichti and Lampard, 2008).

2.4 Self-Calibration Solution

A self-calibration using point targets is performed by simultaneously estimating all model variables (exterior orientation, APs and object point co-ordinates) in a parametric-model, least-squares adjustment with inner constraints imposed on the object points. A minimally-constrained datum is necessary to prevent potential biases in the object point co-ordinates from propagating into other model parameters, particularly the APs. The APs are generally assumed to be block or network invariant. Each group of observations (ρ, θ, α and ω and ϕ) is assigned an a priori variance. Baarda's data snooping is used to identify gross errors and iterative variance component estimation is used to optimise the contribution of each observation group. Additional details about the estimation procedure can be found in Lichti (2007).

2.5 Collimation Axis Error Estimation

In this section the difficulties encountered in the estimation of the collimation axis error b_1 are reviewed. Schneider and Schwalbe (2008) report on the self-calibration of a Riegl LMS-Z210i, a hybrid scanner with a vertical FOV of 80°, conducted as a part of their research on the integration of TLS instruments and other imaging sensors. They report that the collimation axis error b_1 was determined with a low significance level.

Reshetyuk (2006) reports on the self-calibration of three hybrid scanners: a Callidus 1.1, a Leica HDS 2500 and a Leica HDS 3000. He found the collimation axis error b_1 to be very highly correlated (i.e. a coefficient magnitude on the order of 0.99) with the rotation angles. He also found the collimation axis error b_1 estimate to be unreliable for at least one instrument (the Callidus).

Reshetyuk (2009) reports self-calibration results with both simulated and real hybrid scanner data. He used a simulated room having dimensions of 12 m x 9 m x 3 m, which is of similar size to that reported by Lichti (2007) and, coincidentally, that used herein. He simulated data over a near-full vertical FOV and varied the number of scan locations and the number of scans captured at each location, among other factors. His self-calibration adjustments included heavily-weighted a priori parameter constraints on the scanner position and tilt angles (ω and ϕ). One conclusion drawn from the simulations was that the collimation axis error b_1 could not be estimated from only two stations as it was very highly correlated with the κ (tertiary) scanner rotation angle. A second was that the acquisition of nominally orthogonal (in terms of the κ angle) scans from the same location improved the precision of b_1, but did not reduce its correlation with the κ angle. Results from three real dataset self-calibrations are also presented. The κ-b_1 correlation coefficient was 0.99 for both the Callidus and Leica HDS 3000 datasets, but 0.95 for a Leica Scan Station dataset.

Lichti (2007) reports on the calibration of a Faro 880 scanner, which is a panoramic instrument. In this study the angular limits governed by its mode of acquisition (c.f. Table 1) were adhered to. Some of the suggested self-calibration network design measures included the capture of scans from at least two separate locations, the capture of orthogonal scans to de-correlate the APs and the exterior orientation elements and a large elevation range angle to estimate the collimation axis error b_1 as well as the trunnion axis error b_2. No high correlation coefficients between κ and b_1 were encountered; the largest from the ten real datasets tested was 0.22.

The experiments described below have been designed to reveal the impact of angle parameterisation on the b_1-κ functional dependence found by others (e.g., Reshetyuk, 2006, 2009; Schneider and Schwalbe, 2008) and on the precision of b_1, the trunnion axis error b_2 and the vertical circle index error c_0.

3. SIMULATIONS

3.1 Conditions

To study the role of the angle parameterisation, several TLS self-calibration networks were simulated with realistic parameters drawn from the author's past experiences (e.g., Lichti, 2007). First, it was assumed that the calibration would be conducted indoors so the room dimensions were set at 12 m x 9 m x 3 m, which correspond to values from previous experiments with real data. Two nominal scanner locations were set with maximum separation as governed by the room dimensions and the minimum observable range, ρ_0, of 1.5 m, the value of the Faro 880 scanner that has been studied in detail by the author. The simulated room layout is depicted in Figure 1. In all cases the scanner was assumed to be nominally level and the number of orthogonal scans captured from each nominal location was varied.

The number of object points was set to 180, the largest number that was available in previous experiments conducted by the author. Their locations, i.e. whether they were only on the walls or on the walls, the floor and the ceiling, was governed by the permitted range of observations above or below the horizon, denoted by ψ, which was varied from ±10° to ±70°. Note that for a hybrid scanner, ψ directly corresponds to the observed elevation angle (α) range, whereas for a panoramic scanner it corresponds to the limits of α for elevation angles below the zenith and of ($180°-\alpha$) for elevation angles above the zenith.

If the angular range ψ was such that all points were confined to the 4 walls, then the 180 points were distributed in proportion to the respective wall dimensions and uniformly within each wall.

If the angular range ψ was such that points also lay on the floor and ceiling, then one-half of the points were distributed on the 4 four walls as described above and the remaining half were equally divided among the floor and the ceiling. The ceiling and floor point locations were randomly generated subject to the constraint that they could not lie within a certain distance of the instrument location as governed by the minimum observable range ρ_0 and the angular range ψ. This procedure resulted in a distribution of object points that was very realistic.
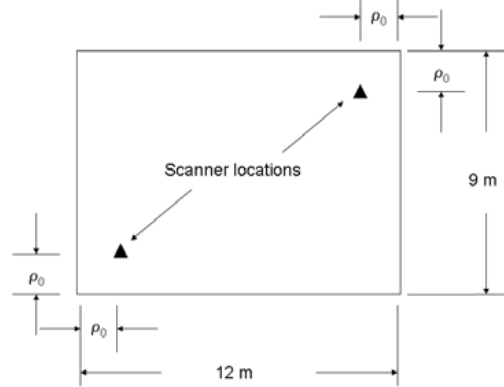
Figure 1. Schematic layout of the simulated room.

The normalised histograms of each observation for a simulated dataset having a full ±70° ψ range and 1440 points are shown on the left side of Figure 2. The corresponding histograms for a real self-calibration dataset of 1135 points are shown on the right side. Both of the horizontal direction histograms are uniformly distributed on (0°, 180°) and both elevation angle histograms comprise lobes centred at 0° and 180° and feature similar, asymmetric shapes. The range-observation histograms differ slightly in shape and the simulated data span a slightly greater range (up to 12.6 m instead of 9.8 m). These differences are of no consequence, though, since a slightly longer maximum range was found to have only a minor impact on the quality of the rangefinder offset a_0 estimation (Lichti, 2007).
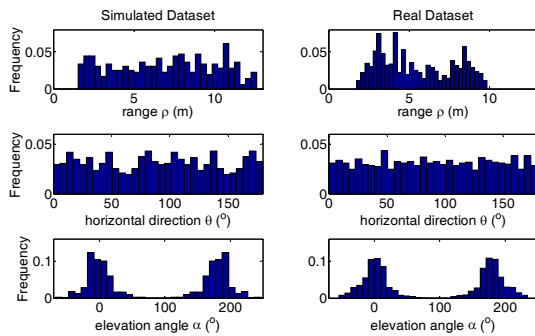

Figure 2. Simulated and real self-calibration dataset histograms of the observations.

Two different simulation cases were studied. The network of Case A comprised four orthogonal scans captured from each of the two instrument locations. The angular range ψ was varied from ±10° to ±70°. For Case B an angular range ψ was set to ±70° and the number of orthogonal scans per instrument location was varied. For both cases, self-calibration adjustments were conducted for both the panoramic and the hybrid angle parameterisations.

Observations were weighted on a group-wise basis using realistic standard deviation estimates from previous experiments. For the range, ρ, the horizontal direction, θ, and elevation angle, α, these values were ±2 mm, ±18″ and ±18″, respectively. Both tilt angle observations' standard deviations were ±3′. No parameter constraints were imposed on the scanner position. The basic AP set comprising a_0, b_1, b_2 and c_0 was used.

3.2 Simulation Case A—Results and Analyses

The propagated standard deviations for selected APs from the simulated self-calibration adjustments as functions of the angular range ψ are shown in Figure 3. Only the angular APs are presented as they constitute the primary focus of this paper. For the panoramic adjustment, the precision of both the collimation axis error b_1 and the vertical circle index error c_0 is independent of the angular range ψ. The precision of the trunnion axis error term b_2 depends strongly on ψ since the tangent function equals zero for horizontal observations and is therefore only weakly estimable when the angular range of observations above and below the horizon is small. AP precision for the hybrid adjustment is much lower than that of the panoramic case, which is the reason for the different y-axis scales of Figure 3. In the hybrid adjustment b_2 and especially b_1 are strongly dependent on the angular range ψ. The precision of b_1 is very large for small values of ψ, which is why its curve disappears from the figure view (σ_{b1}=±1007″ at ψ=±10°). A smaller range was chosen for the y-axis in order for the ψ-dependence of σ_{b2} to be visible. The vertical circle index error c_0 precision is lower than in the panoramic adjustment case and depends on ψ, though not as dramatically as b_1 and b_2. At ψ=±10°, σ_{c0}=±21″ while at ψ=±70° σ_{c0}=±12″.
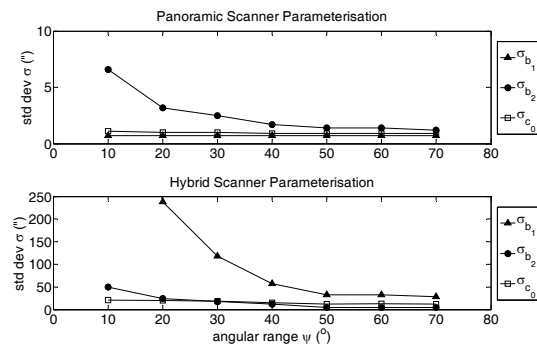

Figure 3. AP precision estimates, simulation Case A. Top: panoramic adjustment. Bottom: hybrid adjustment.
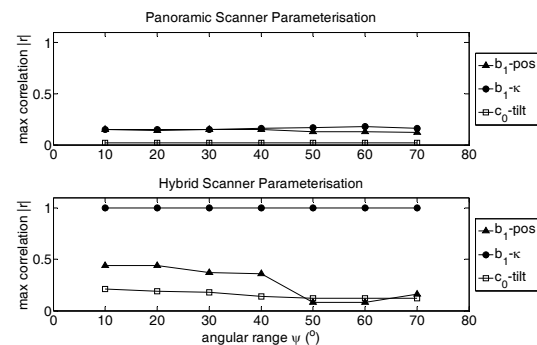

Figure 4. Maximum correlation coefficients, simulation Case A. Top: panoramic adjustment. Bottom: hybrid adjustment.

The maximum correlation coefficient, r, is plotted in Figure 4 for three important pairs of model variables from the simulated

self-calibration adjustments as a function of the angular range ψ: b_1 and the scanner position co-ordinates (denoted pos), b_1 and tertiary angle κ and c_0 and the tilt angles (ω and ϕ). In the panoramic case all three relationships are low (< 0.2) and are independent of ψ. Therefore, these are not of concern. In the hybrid adjustment the problem with this angle parameterisation can clearly be seen as the near-perfect b_1-κ correlation. Interestingly, b_1 and the scanner position elements are correlated (> 0.4) for low values of ψ, but the dependence drops to below 0.2 at ±50°. The other correlation mechanism are low and, thus, not of concern. The b_2 parameter was not correlated with any position or orientation elements.

In another test the collimation axis error b_1 was removed from the AP set and the hybrid-model simulations were performed again. Omission of this parameter has no effect on the precision of b_2 and c_0, indicating that their estimation is governed primarily by observation geometry. Thus, one can expect inherently less precise angular AP estimates for the hybrid model than for the panoramic model.

3.3 Simulation Case B—Results and Analyses

The AP precision estimates for both the panoramic and hybrid self-calibration adjustments are plotted in Figure 5 as a function of the number of orthogonal scans captured at each simulated instrument location (i.e. Case B). For the panoramic scanner a large improvement is realised for all three angular APs by adding a second, orthogonal scan. The greatest gain is in σ_{b2}, which improves by an order of magnitude from ±15″ to ±1.7″, whereas σ_{b1} and σ_{c0} improve by factors of 4 and 2.5, respectively. The improvement gained by adding a third and a fourth orthogonal scan is lower, in proportion to the square root of the number of observations. For the hybrid adjustment case the precision improvement gained by adding one or more orthogonal scans is only that due to the corresponding increase in the number of observations, i.e. in proportion to the square root of the number of observations.
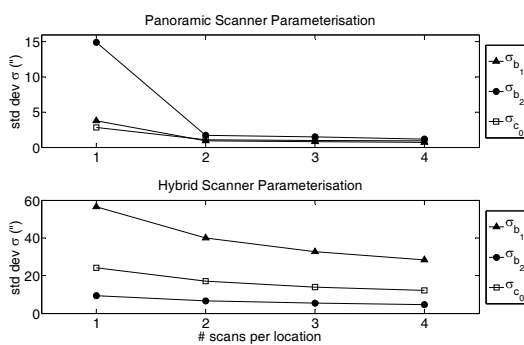

Figure 5. AP precision estimates, simulation Case B. Top: panoramic adjustment. Bottom: hybrid adjustment.

The maximum correlation coefficients between selected APs and exterior orientation parameters for both the panoramic and hybrid self-calibration adjustments as a function of the number of orthogonal scans are shown in Figure 6. While there is no improvement gained by increasing the number of orthogonal scans in the hybrid case, there is improvement in the panoramic adjustment. The correlation between b_1 and the exterior orientation is as high as 0.64 for a single scan per instrument location, but drops to 0.21 or less when one or more orthogonal scans are added to the network.
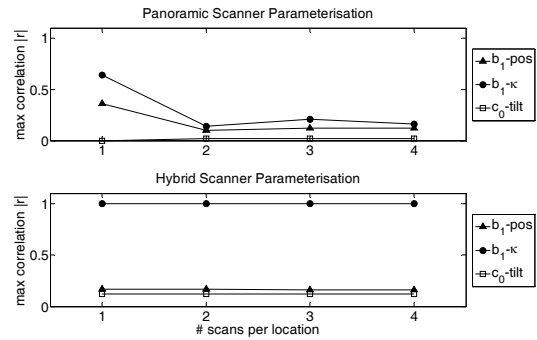

Figure 6. Maximum correlation coefficients, simulation Case B. Top: panoramic adjustment. Bottom: hybrid adjustment.

3.4 Simulation Summary

To summarise the outcomes of simulation Case A, the high b_1-κ correlation found by others (e.g., Reshetyuk, 2006, 2009; Schneider and Schwalbe, 2008) stems from the use of the hybrid angle parameterisation, which was the logical choice for their studies since hybrid instruments were tested. A large range of elevation angle observations in one "layer", as is captured by a hybrid scanner, is not sufficient for reliable estimation of b_1 from 2 scanner locations. This is in agreement with the findings of Reshetyuk (2009). However, if the angular range ψ spans two layers, as in the case of a panoramic scanner, then b_1 is estimable from only two locations. In this case the angular range ψ need not be large for precise b_1 or c_0 estimation, but should be large for precise b_2 estimation.

From Case B it was found that, as Reshetyuk (2009) reported, no improvement to the estimation of b_1 in terms of reduced parameter correlation is gained by including at least two orthogonal scans in a hybrid scanner self-calibration network. For a panoramic scanner self-calibration adjustment, though, considerable gains are made by including at least two orthogonal scans in the network: the b_1-κ angle correlation is greatly reduced and the angular AP precision is improved beyond the factors expected from basic statistics, i.e. the reciprocal of the square root of the number of observations.

4. REAL DATASETS

4.1 Description

To support the simulation outcomes, results from a real self-calibration dataset are presented. The data were captured with a Faro 880 terrestrial laser scanner, a panoramic instrument that features a vertical FOV of 320° (−70° to 250°) and a 180° horizontal FOV. Its rangefinder operates by the phase difference method in which the range is proportional to the phase difference between the received and emitted signals. It also features two orthogonal inclinometers that measure the instrument's tilt. Their outputs are used by the accompanying software to correct the captured scan data, resulting in a 'levelled' dataset, which justifies the use of zero-valued ω and ϕ parameter observations (i.e. Equations 5 and 6).

The target field comprised an array of 131 proprietary Faro targets arranged on the walls, the floor and the ceiling of a 12 m x 9 m x 3 m room. Scans were captured from two nominal locations on opposite sides of the room separated by 6.7 m. A

series of four scans were captured at each location. For each scan the entire instrument was rotated about its vertical axis atop the tripod so as to introduce a 90° κ rotation angle relative to the previous scan. More details about the experiment data capture can be found in Lichti (2007).

The full dataset comprised a total of 2209 observations, including the 16 inclinometer parameter observations. The basic AP set described herein was estimated in the free-network self-calibration adjustment and the resulting redundancy was 1768. The range of data of the complete dataset of 8 scans spanned 8.7 m in range ρ, 179° in horizontal direction θ and the angular range ψ of observations above and below the horizon was ±76°.

The first set of results closely corresponds to simulation Case A with $\psi = \pm 70°$. The full dataset was adjusted using both the panoramic angle parameterisation and the hybrid parameterisation. Strictly speaking the latter is incorrect for this type of scanner but it was used to confirm the simulation outcomes. The second set of results corresponds to simulation Case B. Using the panoramic angle parameterisation, the self-calibration adjustment was performed with a variable number of orthogonal scans (1, 2, 3 or 4) at each location.

4.2 Results

The real-data self-calibration quality measures for the collimation axis error b_1, the angular AP most affected by the angle parameterisation, are presented in Table 2. For Case A, it can be seen from the poor precision of b_1 and the near-perfect b_1-κ correlation that reliable estimation of b_1 is not possible from two scanner locations when the hybrid angle parameterisation is used. However, reliable b_1 estimation is possible for the panoramic case as the two variables are almost completely de-correlated and the precision is much higher. Thus, these outcomes confirm the findings of simulation Case A.

For Case B, the benefit of adding orthogonal scans to the self-calibration network when the panoramic angle parameterisation is used is evident in the reduction of the b_1-κ correlation from 0.87 to 0.10 and the order-of-magnitude improvement in σ_{b1} from ±12.7″ to ±1.2″. Therefore, these outcomes confirm the findings of simulation Case B.

Case	σ_{b1}	Maximum $|r_{b1-\kappa}|$
Real Data Case A		
Panoramic self-calibration	±1.2″	0.10
Hybrid self-calibration	±78.2″	1.00
Real Data Case B		
1 scan per station	±12.7″	0.87
2 orthogonal scans per station	±2.3″	0.28
3 orthogonal scans per station	±1.5″	0.17
4 orthogonal scans per station	±1.2″	0.10

Table 2. Real data results for the different angle parameterisations and variable number of scans.

5. CONCLUSIONS

In this paper the role of angle parameterisation, specifically the allowable limits of the horizontal direction and elevation angle in the self-calibration of TLS instrument has been examined. Results from both simulated and real-data experiments show that the reliable estimation of the collimation axis error b_1 is

possible for panoramic scanners but is not for hybrid scanners due to its very high correlation with the κ rotation angle. Estimation of b_1 from only two instrument locations is possible for the panoramic scanner parameterisation and the inclusion of multiple, nominally-orthogonal scans improves the solution in terms of reduced b_1-κ angle correlation as well as improved angular AP precision. Due to the low reliability of its estimation in hybrid self-calibration, b_1 should be omitted from the additional parameter model unless the κ can be independently observed. Since only the ω-ϕ-κ rotation angle sequence has been studied herein, further investigation is required to determine if other rotation angle parameterisations (e.g. quaternion) are subject to the same correlation issues.

REFERENCES

Abmayr, T., Dalton, G., Hätrl, F., Hines, D., Liu, R., Hirzinger, G., Frölich, C., 2005. Standardization and visualization of 2.5D scanning data and color information by inverse mapping. *Optical 3-D Measurement Techniques VII*, Vienna, Austria, 3–5 October, 2005, vol. I, 164–173.

Bae, K.-H. and Lichti, D.D, 2007. On-site self-calibration using planar features for terrestrial laser scanners. *The International Archives of the Photogrammetry, Remote Sensing and Spatial Information Sciences*, 36 (Part 3/W52), 14-19.

Dorninger, P., Nothegger, C., Pfeifer, N. Molnár, G., 2008. On-the-job detection and correction of systematic cyclic distance measurement errors of terrestrial laser scanners. Journal of Applied Geodesy, 2 (4), 191–204.

Gielsdorf, F., Rietdorf, A., Gruendig, L., 2004. A concept for the calibration of terrestrial laser scanners. *Proc. FIG Working Week*, Athens, Greece, 22–27 May 2004. On CD-ROM.

Lichti, D.D. and Lampard, J., 2008. Reflectorless total station self-calibration. *Survey Review*, 40 (309), 244-259.

Lichti, D.D., 2007. Modelling, calibration and analysis of an AM-CW terrestrial laser scanner. *ISPRS Journal of Photogrammetry and Remote Sensing*. 61 (5), 307-324.

Point of Beginning (POB), 2009. 2009 laser scanner survey. http://laser.jadaproductions.net/. Last accessed 4 Feb. 2009.

Reshetyuk, Y., 2006. Calibration of Terrestrial Laser Scanners Callidus 1.1, Leica HDS 3000 and Leica HDS 2500. *Survey Review*, 38 (302), 703-713.

Reshetyuk, Y. 2009. Self-calibration and direct georeferencing in terrestrial laser scanning. Doctoral Thesis. Department of Transport and Economics, Division of Geodesy, Royal Institute of Technology (KTH), Stockholm. Sweden, January.

Schneider, D. and Schwalbe, E., 2008. Integrated processing of terrestrial laser scanner data and fisheye-camera image data, *The International Archives of the Photogrammetry, Remote Sensing and Spatial Information Sciences,* 37 (Part B5), 1037-1043.

Staiger, R., 2003. Terrestrial laser scanning – technology, systems and applications. In: *Proc. of 2nd FIG Regional Conference, Marrakech*, Morocco, 2 – 5 December, http://www.fig.net/pub/morocco/index.htm. Last accessed 2 Feb. 2009.